Water Practice & Technology

IWA PUBLISHING

Water Practice & Technology Vol 19 No 3, 824 doi: 10.2166/wpt.2024.022

Green synthesis, characterisation, and performance evaluation of ZnO/TiO_2 nanocomposite for cationic and anionic dye removal from aqueous solutions under solar irradiation

Kavya Anil and Anupama Surenjan *

Department of Civil Engineering, National Institute of Technology-Karnataka, Surathkal, Mangaluru 575025, India
*Corresponding author. E-mail: anupama@nitk.edu.in

AS, 0000-0003-2441-0605

ABSTRACT

Utilising plant extract for the synthesis of nanocomposite shows great potential as a viable substitute for conventional chemical method. In this study, ZnO/TiO_2 composite of three different weight ratios (1:2, 1:1, and 2:1) were green synthesised using hibiscus leaf extract as the capping agent. The synthesised composites were characterised using X-ray Diffraction (XRD), Field Emission Scanning Electron Microscopy (FESEM), UV–Vis Diffuse Reflectance Spectroscopy (UV–Vis DRS), Energy Dispersive X-ray Spectrometer (EDS), and Fourier Transform Infrared Spectroscopy (FTIR). XRD results confirmed the presence of wurtzite ZnO and anatase TiO_2 in the composite. FTIR and FESEM analysis confirmed the formation of the composite. The composite was used for the removal of methylene blue and methyl orange dye under solar radiation. The degradation rate constant (*k*) of the composite with 1:2 weight ratio was 1.9 times *the k* value of pure TiO_2. The effect of photocatalyst amount, initial pH of the dye solution, and reusability of the catalyst was investigated. The TiO_2 and ZnO/TiO_2 samples indicated a bandgap of 3.14 and 2.98 eV, respectively, which suggests better photocatalytic activity and also making the composite more active in the visible region.

Key words: composite, dye removal, green synthesis, heterojunction, photocatalysis

HIGHLIGHTS

- ZnO/TiO_2 nanocomposite has been synthesised through green synthesis using hibiscus leaf extract as the capping agent.
- UV–Vis study revealed a bandgap of 2.98 eV, with a red shift in absorption spectrum.
- Optimisation study of catalyst dosage and pH for maximum degradation efficiency for dyes were carried out.
- ZnO/TiO_2 (1:2) composite exhibited good recyclability up to three cycles of treatment.

GRAPHICAL ABSTRACT

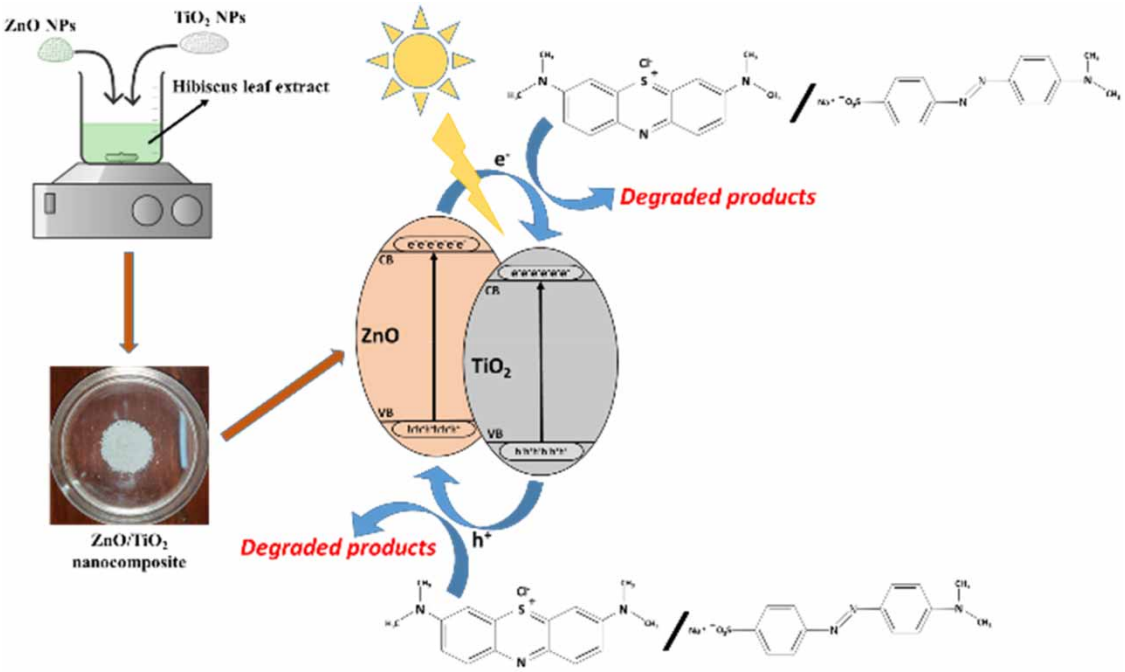

1. INTRODUCTION

Textile industry uses numerous dyes in various phases of the manufacturing process to impart desired striking colours to their products. These dyes do not adhere to the fabric tightly and during the washing stage, excess of these dyes are discharged into the industrial wastewater. As a result, textile wastewater comprises excess of organic pollutants, toxic metals, and residual dyes. These treated effluents are discharged into the aquatic environment such as lakes, rivers, ponds, and streams adding to the water pollution (Chandrabose *et al.* 2021). Dye effluents increase the biological and chemical oxygen demand of water. They also contain large amounts of organic, inorganic, and toxic substances in it which persist in the water bodies for a very long time posing serious threats to the environment. Dyes impart intense colour to the water streams preventing the penetration of sunlight, and reducing photosynthetic activity, which results in the development of anoxic conditions for flora and fauna (Al-Tohamy *et al.* 2022). Methylene blue (MB) dye and methyl orange (MO) dyes are one of the most commonly used dyes worldwide (Mehrabi & Javanbakht 2018). Figure 1(a) and 1(b) depicts the chemical structure of MB and MO, respectively. Because of their aromatic structure and xenobiotic properties, these dyes are stable, non-biodegradable, carcinogenic, and toxic which requires concerted efforts for removal and degradation. The conventional treatments such as coagulation, sedimentation, adsorption, filtration, and membrane processes are ineffective in degrading these compounds and have high maintenance costs which call for the need for a green technology that can completely degrade the toxic pollutants to non-toxic substances. The advanced oxidation process (AOP) is a sustainable technology that degrades pollutants into thermodynamically stable oxidation products such as water, carbon dioxide, and other non-toxic substances using reactive oxygen species such as hydroxyl radicals (Mehrabi & Javanbakht 2018). Photocatalysis is an irradiation AOP that generates electron/hole pair when a semiconductor is exposed to light having energy more than the bandgap of the catalyst. The electron reduces the acceptor molecule and the hole oxidises the donor molecule, creating a redox environment simultaneously (Rashid Al-Mamun *et al.* 2022). The rapid industrial growth has also led to

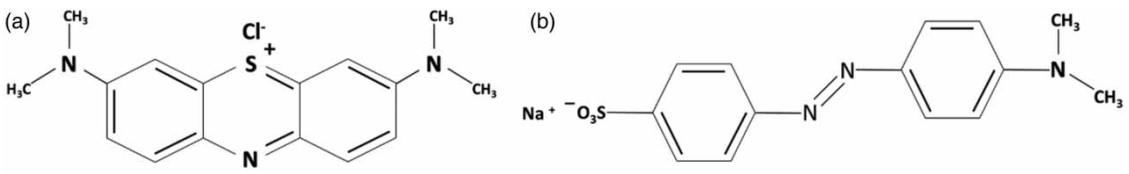

Figure 1 | Chemical structure of (a) methylene blue and (b) methyl orange.

rapid depletion of natural energy sources and increased pollution. The need for clean and renewable energy solutions has become crucial. Photocatalyst offers a potential solution, on exposure to sunlight they absorb solar energy to produce hydrogen (H_2) from photocatalytic water splitting and also degrade organic pollutants, promising a cleaner environment and sustainable energy. Therefore, wastewater treatment using photocatalysis under solar radiation is likely the most promising application of AOP (Fendrich *et al.* 2018). TiO_2 and ZnO are the most widely used catalyst in photocatalysis because of their stability, ease of preparation, non-toxicity, and flexibility. TiO_2 and ZnO have a similar bandgap of 3.2 eV making them active only in the UV region which comprises only 4% of the solar spectrum (Ali *et al.* 2021). Since both catalysts have similarities in their conduction band (CB) and valence band (VB), coupling these semiconductors will make the transfer of electrons and holes more easily reducing their recombination. Moreover, ZnO is one of the main semiconductors used for synthesising visible light-active-catalysts (Moradi *et al.* 2016). The composite formation will help reduce the bandgap, allowing the photocatalyst to absorb a broader range of visible light, which constitutes a significant part of solar radiation. This increased absorption efficiency can lead to improved photocatalytic activity. The composite was reported to show better photodegradation efficiency due to the synergic effect of both catalysts (Bai *et al.* 2021). Figure 2 illustrates the scheme of mechanism of ZnO/TiO_2 nanocomposite under solar radiation. There are different methods for the synthesis of nanocomposites. Conventional fabrication of nanoparticles involves a wet chemical method that uses toxic and environmentally unfriendly chemical precursors (Tumbelaka *et al.* 2022). Whereas green synthesis uses natural ingredients such as plant extract for the fabrication of nanoparticles. Green synthesis has the advantage of not using toxic chemicals, standard acid/base compounds, or elevated temperatures. Green synthesised nanoparticles are far superior to those manufactured chemically or physically due to better control over the size and shape of nanoparticles. Green synthesis is an energy-saving, simple, and cost-effective method that can be used for the large-scale production of nanoparticles. The current study uses *Hibiscus rosasinensis* leaf extract as the capping agent for the green synthesis of nanocomposite. Hibiscus leaves contain a large amount of phenolic compounds and bioactive components which are required for the in situ reduction and stabilisation of nanoparticles. These phytochemicals present in the leaf extracts act as a capping agent that stabilises the interface where nanoparticles interact with their preparation medium. They inhibit the overgrowth of nanoparticles and prevent their agglomeration in colloidal synthesis (Soto-Robles *et al.* 2019).

The study investigates the photocatalytic activity of green synthesised ZnO/TiO_2 nanocomposites using hibiscus leaf extract. The synthesised nanocomposite was used to degrade cationic dye and anionic dye in an aqueous

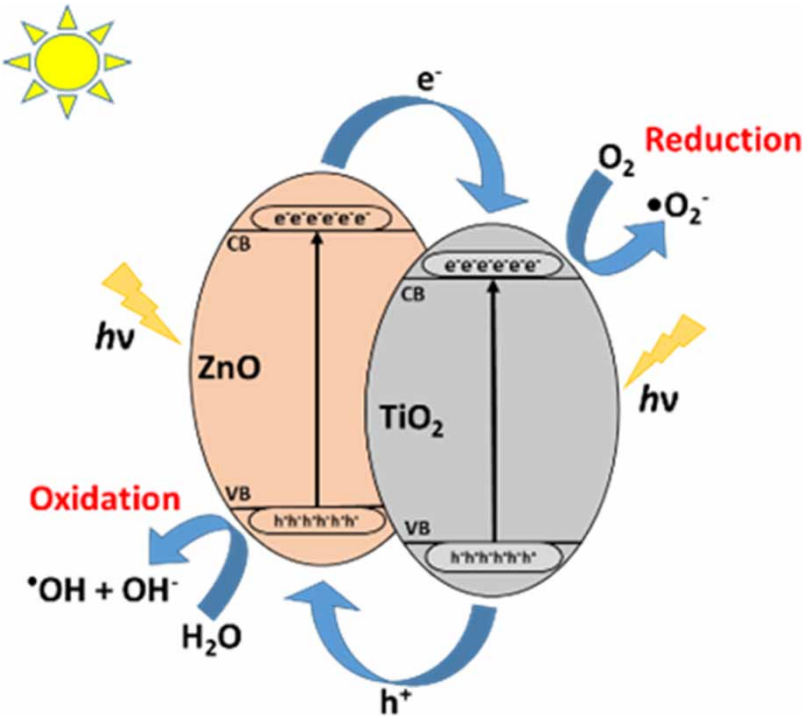

Figure 2 | Proposed photocatalytic mechanism and electron transfer in ZnO/TiO_2 composite under solar radiation.

solution by solar radiation. The effect of different ZnO molar ratios on the characterisation and photocatalytic behaviour of the nanocomposite was studied. In addition, factors affecting the degradation of dyes, including different concentrations of catalyst and pH of the solution were investigated. Reusability study of the catalyst was also carried out to investigate the stability of the catalyst.

2. MATERIALS AND METHODS

2.1. Materials

Hibiscus leaves were collected from the National Institute of Technology, Karnataka campus. The chemicals used in the study were titanium tetraisopropoxide (TTIP) (99%), ethanol (96%), zinc nitrate ($ZnNO_3$) (99%), TiO_2 (99%), MB powder (85%), and MO powder (85%). The pH of the aqueous solutions was adjusted using solutions of 2 N NaOH and 1 N H_2SO_4. Double distilled water was used for the preparation of leaf extract and all other solutions. All the chemicals used were of analytical grade and were not further purified.

2.2. Green synthesis of ZnO/TiO_2 nanocomposite

2.2.1. Preparation of hibiscus leaf extract

A sufficient quantity of hibiscus leaves was gathered from the NITK campus. The leaves underwent multiple rinses with distilled water to eliminate any dirt or dust particles and were subsequently air dried. 50 g of the cleaned leaves were added to 500 mL of double distilled water and boiled at 100 °C until the colour of the solution changed to yellow. The prepared extract was then allowed to cool. Once cooled, the prepared extract was filtered using Whatman filter paper grade no. 1, pore size of 11 μm.

2.2.2. Synthesis of TiO_2 nanoparticles using hibiscus leaf extract

A solution of 7.55 mL TTIP and 92.45 mL of ethanol was poured into a glass beaker. To this solution, 30 mL of distilled water and 15 mL of hibiscus leaf extract were added dropwise with continuous mixing at room temperature for 4 h. The mixture obtained after stirring was washed several times with distilled water and filtered using vacuum filtration. The yellow colour thick paste obtained was kept overnight in air-heated oven at 110 °C. The solid TiO_2 was then calcined at 570 °C for 3 h in a muffle furnace.

2.2.3. Synthesis of ZnO nanoparticles using hibiscus leaf extract

The composites in the present study were synthesised using a previously established method (Abd El-Kader *et al.* 2021) with modifications. 30 mL of the previously prepared hibiscus leaves extract was taken in a glass beaker and heated at 70 °C. 11 g of $ZnNO_3$was added step-by-step to the solution with continuous stirring for 90 min until a deep yellow colour paste was formed. The paste was then collected in a crucible and burned for 2 h at 450 °C in a muffle furnace. A light-yellow powder obtained after burning was ground using a mortar and stored in an air-tight container.

2.2.4. Synthesis of ZnO/TiO_2 nanocomposite using hibiscus leaf extract

About 18.1 mL of hibiscus leaf extract was heated at 700 °C. To this solution, 1.8 g of both previously prepared TiO_2 and ZnO nanoparticles were added together with continuous mixing until a greyish-white paste was obtained. The paste was collected in a crucible and heated at 700 °C for 3 h in a muffle furnace. The obtained ZnO/TiO_2 nanocomposite of the ratio 1:1 was ground using a mortar and stored in an air-tight container for characterisation and further experiments. Similarly, ZnO/TiO_2 nanocomposite of different ratios (1:2 and 2:1) was prepared by varying the weight concentrations of ZnO and TiO_2 (Abd El-Kader *et al.* 2021). In the following sections ZnO/TiO_2 of ratio 1:1, 1:2, and 2:1 is abbreviated as Z1T, ZT2, and Z2T, respectively, and bare TiO_2 as T.

2.3. Characterisation

Fourier Transform Infrared Spectroscopy in the range 400–4,000 cm^{-1} (FTIR, Spectrum 2 FTIR Spectrometer, PerkinElmer, Singapore) was carried out to investigate molecular vibrations and functional groups present in the catalyst. The crystal structure and phase of the catalyst were identified with the help of X-ray Diffraction (XRD, Empyrean 3rd Gen, Malvern PANalytical, Netherlands) using Cu-Kα radiation (Shimadzu, XD-3 H) in the diffraction angle (2θ) range of 20°–80° with 10°/min scanning speed. Energy Dispersive X-ray Spectrometer (EDS; Octane Elite, EDAX AMETEK) in conjunction with FESEM was used to determine elemental composition. The surface morphology and shape of the catalyst were determined using High-Resolution Field Emission Scanning Electron Microscopy (HR-FESEM, GEMINI 300, Carl Zeiss, Germany). The absorbance

and bandgap energy of the catalyst were determined using UV–Vis Diffuse Reflectance Spectroscopy (UV–Vis DRS, Lambda 950, Perkin Elmer, Singapore).

2.4. Solar photocatalytic activity evaluation

MB and MO dyes were used as model pollutants for evaluating the photocatalytic activity of the nanocomposite. Photodegradation of the dyes was carried out in a cylindrical glass reactor of 200 mL volume covered with a glass plate along with magnetic stirring. The setup was placed on the roof of the Civil Department block (13 °00′43″ N 74 °47′38″ E) in the NITK campus. According to National Solar Radiation Database, the average global horizontal solar irradiance in Surathkal was 6–6.5 kWh/m^2/day for a period of 4 months from January 2023 to April 2023. The source of light used throughout the experiments was solar radiation. The experiments were carried out from 10 am to 4 pm as maximum sunlight was received during these hours. In a typical experiment, 10 mg of the catalyst was dispersed in 100 mL of 8 mg/L dye solution. Before irradiation, the solution was kept in the dark for 30 min to achieve adsorption–desorption equilibrium. The suspension containing the dye and photocatalyst was exposed to sunlight to initiate the photocatalytic reaction. The timing of the photocatalytic reaction commenced with the onset of sunlight exposure. During the reaction, the mixture was stirred using magnetic stirrer. For the kinetic studies, 5 mL of aliquots were withdrawn at regular intervals of time. The collected samples were centrifuged at 3,000 rpm for 10 min to remove the catalyst particles. The concentration of MB and MO was determined by checking their absorbance at a wavelength of 664 and 464 nm, respectively, using a UV–Vis spectrophotometer. The dye decolourisation efficiency was calculated as follows,

$$\text{Decolourisation efficiency } (\%) = \left(1 - \frac{C_0}{C_t}\right) \times 100 \tag{1}$$

where C_0 represents the initial concentration of the dye solution and C_t represents the concentration of dye solution after t minutes.

The kinetics of photocatalytic effect of ZnO/TiO_2 nanocomposite on the degradation rate of MB and MO dye was studied with the help of pseudo-first-order Langmuir–Hinshelwood model as represented in Equation (2)

$$-ln\left(\frac{C}{C_0}\right) = kt \tag{2}$$

where C_0 is initial dye concentration and C is the concentration after reaction time t, k is the rate constant (Sadiq *et al.* 2021).

3. RESULTS AND DISCUSSION

3.1. Characterisation of the nanocomposites

To identify the crystal structure and phase of the synthesised catalyst, XRDanalyses were carried out. The XRD patterns of ZnO/TiO_2 composites of different ratios and TiO_2 are depicted in Figure 3. The intense peaks at the planes of (100), (002), (101), (102), (110), (103), (200), (112), (201), and (004) with the 2θ values of 31.75°, 34.41°, 36.24°, 47.53°, 48.03°, 56.58° 62.80°, 66.35°, 67.93°, 70.27°, and 72.67°, respectively, represented the hexagonal wurtzite structure of ZnO (JCPDS card no. 01-075-0576) and also the peak planes (101), (103), (004), (112), (200), (105), (211), (213), (216), and (220) of 2θ values 25.29°, 36.94° 37.79° 38.56° 48.03° 53.88° 55.05° 62.09° 68.98°, and 72.56°, respectively, represented the anatase phase of TiO_2 (JCPDS card no. 01-072-7058). The composite consists of both anatase TiO_2 and wurtzite ZnO which can be seen in the XRD patterns. There were no impurity peaks in the observed XRD pattern indicating that the synthesised catalysts were pure. Strong diffraction peaks of ZnO can be seen in the composites with its intensity increasing with an increase in ZnO concentration. As the TiO_2 content increases the corresponding peaks of ZnO shifted to a higher 2θ value due to ionic radii mismatch between Zn^{2+} (0.75 Å) and Ti^{4+} (0.61 Å) (Ali *et al.* 2021). The crystallite size of the specimens was measured using Debye Scherer Formula (Ali *et al.* 2021).

$$D = \frac{K\lambda}{\beta \cos\theta}$$

where β stands for Full Width at Half Maxima (FWHM) of the peak, K corresponds to shape factor (~0.94 for spherical shape), λ belongs to the wavelength of Cu-K_α radiation (1.54 Å) and θ stands for the Bragg angle,

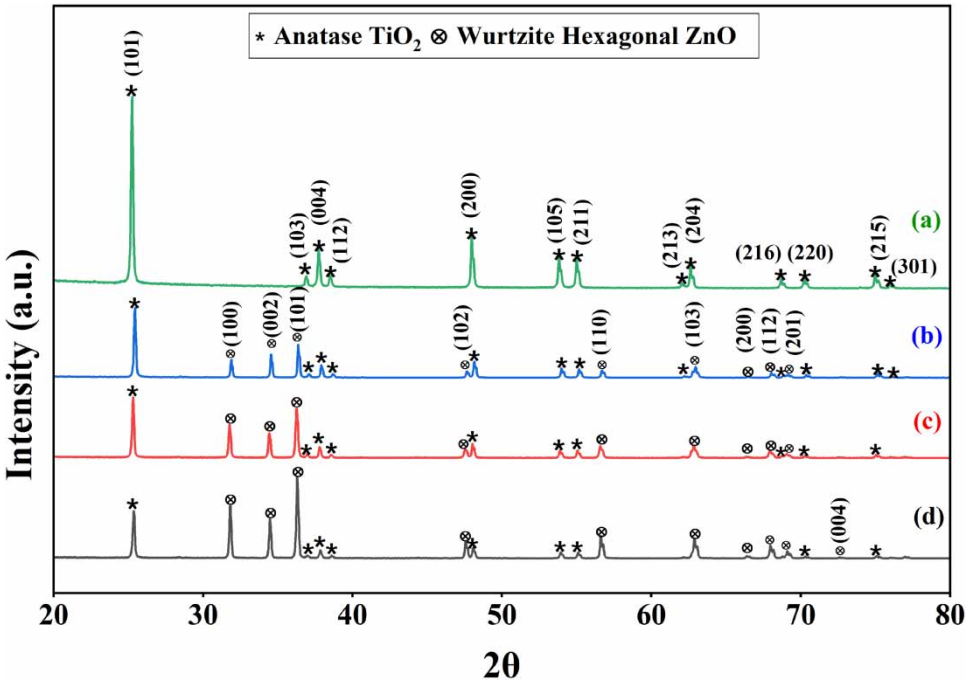

Figure 3 | XRD patterns of (a) TiO_2; (b) ZnO/TiO_2 (1:2); (c) ZnO/TiO_2 (1:1); and (d) ZnO/TiO_2 (2:1).

respectively. The average crystallite size of the composites ZnO/TiO_2 (2:1) (Z2T), ZnO/TiO_2 (1:1) (Z1T), and ZnO/TiO_2 (1:2) (ZT2) were 111.9, 90.47, and 86.38 nm, respectively.

FTIR spectrum provides information about molecular vibrations and functional groups present in the materials. FTIR spectra were recorded between 400 and 4,000 cm^{-1}. FTIR analyses of ZT2 and singlet materials are presented in Figure 4. The broad band observed at 3,200–3,570 cm^{-1} denotes the hydroxyl group, H-bonded (Nandiyanto *et al.* 2019) and the small peak at 1,635 cm^{-1} in ZT2 and 1,637 cm^{-1} in TiO_2 and ZnO might be due to the surface adsorbed water. This hydroxyl group is assumed to be responsible for the photocatalytic

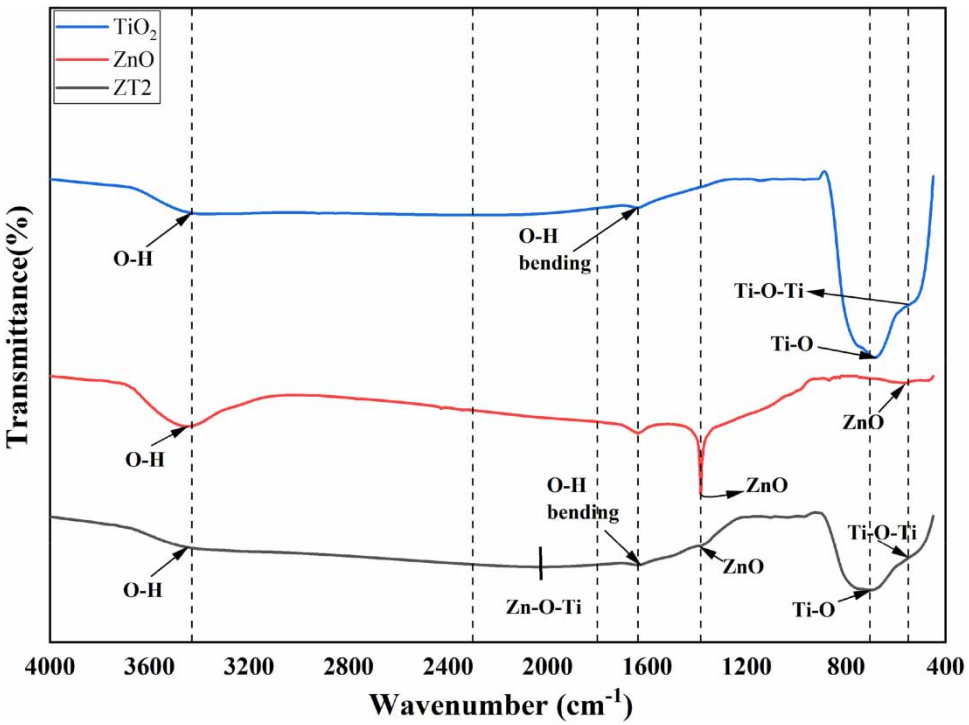

Figure 4 | FTIR spectra of TiO_2, ZnO, and ZnO/TiO_2 (1:2).

activity (Sethy *et al.* 2020). The two transmittance peaks at 550 and 704 cm^{-1} are attributed to the stretching vibrations of Ti–O–Ti and Ti–O (Nam *et al.* 2012). This indicates the presence of TiO_2 structure. The FTIR spectrum, absorption at 400–700 cm^{-1} centred at 566 cm^{-1} could be attributed to ZnO stretching mode (Mbrouk *et al.* 2022) which confirms the formation of ZnO using hibiscus leaf extract. A characteristic band at 1,384 cm^{-1} attributed to ZnO, indicating the presence of ZnO in the catalyst (Mousa *et al.* 2021). Also, the broad band between 1,800 and 2,300 cm^{-1} centred at 2,028 cm^{-1} indicate the vibration mode of Zn–O–Ti this implies that zinc (Zn), oxygen (O), and titanium (Ti) atoms are involved in the bonding (Akhter *et al.* 2023). The bonding could occur through the sharing or transfer of electrons between these elements. The Zn–O–Ti bond might suggest ZnO has been incorporated or embedded into the surface of TiO_2. The absorption peak at 1,100 cm^{-1} could be attributed to the functional group of flavonoids present in the hibiscus leaf extract (Ma *et al.* 2015) which confirms that the nanocomposite has been synthesised utilising hibiscus leaf extract as a bio-reductant.

The morphological analysis of ZnO, TiO_2, and ZnO/TiO_2 (ZT2) composite was investigated through FESEM analysis. SEM imaging of ZnO in Figure 5(a) and 5(b) shows a flaky agglomerated hexagonal structure

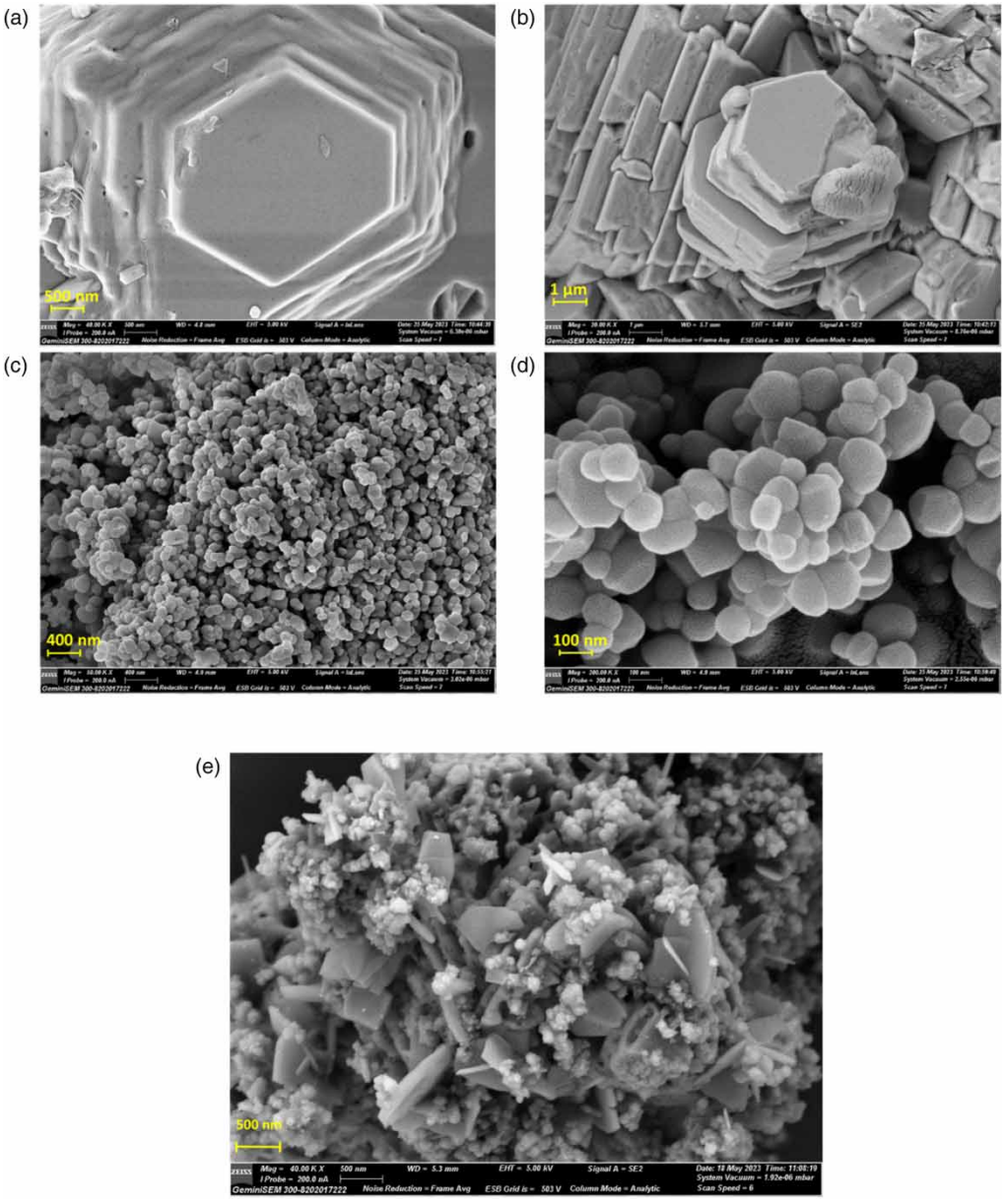

Figure 5 | SEM images of (a) and (b) ZnO; (c) and (d) TiO_2 and (e) ZT2 composite.

conforming to the wurtzite structure of ZnO supporting the XRD results (Jayappa *et al.* 2020). The agglomeration of the particle might be due to the use of heat in the electric furnace that gives the crystalline structure (Sadiq *et al.* 2021). SEM micrographs of anatase TiO_2 as shown in Figure 5(c) and 5(d) depict the semi-spherical structure and rough surfaces. Figure 5(e) shows ZnO/TiO_2 (ZT2) composite. It can be seen that ZnO particles were formed on the TiO_2 spheres. To confirm the elemental composition of ZnO/TiO_2 (ZT2) composite EDS analysis was carried out. Figure 6 clearly shows the peaks of Ti, Zn, and O atoms and gives their atomic ratios. The EDS analysis confirms the presence Ti, O, and Zn atoms in the spectra. No other peaks were observed in the EDS analysis which confirms the absence of any impurities in the ZT2 composite.

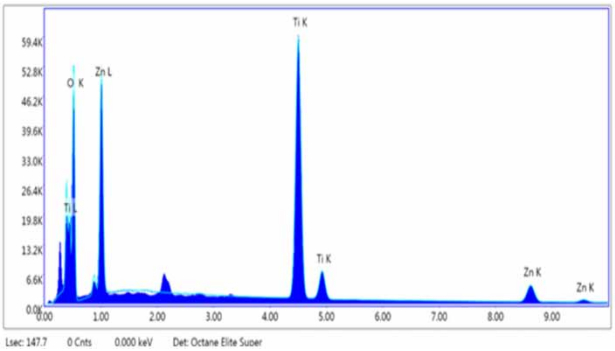

Element	Weight %	Atomic %	Net Int.	Error %
O K	32.53	61.18	1739.10	9.78
TiK	46.26	29.06	4681.90	1.98
ZnK	21.21	9.76	408.30	4.19

Figure 6 | SEM-EDS elemental mapping of ZT2 composite.

UV–Vis absorption spectra of TiO_2 and ZT2 are shown in Figure 7(a). From the UV–Vis DRS, it can be noted that the composite ZT2 has a red shift compared to TiO_2 indicative of its activity shifting to the visible region of the light spectrum (Akhter *et al.* 2023). The composite's absorption peak is approximately 381 nm, whereas TiO_2 has an absorption peak of around 350 nm. Figure 7(b) shows the Tauc plot of bare TiO_2 and the composite. Tauc plot was made from UV–Vis data to calculate the direct bandgap of as synthesised TiO_2 and ZT2 composite. The bandgaps of the samples were calculated by extrapolation of $(\alpha h\nu)^2$ vs. photon energy ($h\nu$), where α is the absorption coefficient and $h\nu = (1{,}240/\lambda)$ eV. The absorption energy, which relates to a bandgap, is obtained by extrapolating the value of $h\nu$ to $\alpha = 0$. The bandgap energy (E_g) of TiO_2 was 3.14 eV which is very close to the reported bandgap of anatase TiO_2 (3.2 eV) (Mousa *et al.* 2021). The composite ZT2 yields a bandgap of 2.98 eV. This reduction in the bandgap might be due to the formation of heterojunction between ZnO and TiO_2. Formation of heterojunctions may lead to (i) mixing of energy band levels; (ii) interfacial coupling effect between different phases like anatase TiO_2 and wurtzite ZnO; and (iii) different band edge positions of the semiconductors (Kumari *et al.* 2022). The bandgap energy of the composite is lower than that of TiO_2 prepared under the same conditions which could also be attributed to the synergistic effect between the CB of TiO_2 and ZnO

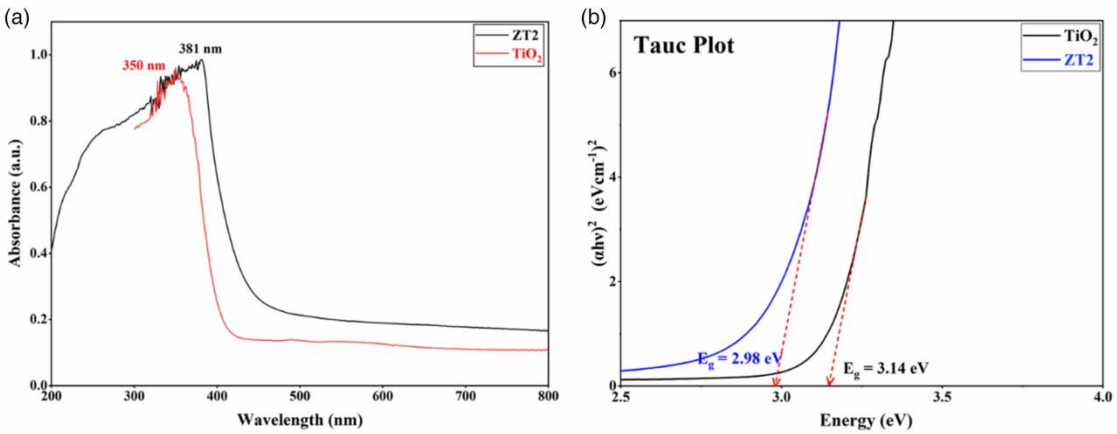

Figure 7 | (a) UV–Vis DRS of TiO_2 and ZT2 (b) Tauc plot of TiO_2 and ZT2.

(Mbrouk *et al.* 2022). It was reported that catalysts with lower bandgap energy showed better photodegradation of organic dye compounds (Rashid Al-Mamun *et al.* 2022).

3.2. Solar photocatalytic studies

3.2.1. Effect of different weight ratios of ZnO/TiO_2 on photocatalytic degradation

MB dye was used as the model pollutant to study the effect of the ZnO/TiO_2 weight ratio on the photocatalyst. In Figure 8, it can be observed that after 150 min of contact time, ZnO/TiO_2 (1:2) (ZT2) photocatalyst showed the highest efficiency among all the catalysts with an efficiency of 96.13% which fallout after 150 min of contact time followed by the ZnO/TiO_2 (1:1) (Z1T) having an efficiency of 89.73%. Both composites showed better efficiency than green synthesised TiO_2. Table 1 shows the kinetic data of photocatalytic degradation. ZT2 has a degradation rate constant of 0.02362 min^{-1} which is 1.9 times the degradation rate constant of green synthesised TiO_2. This might be due to the formation of heterojunction between ZnO and TiO_2 composite (Kumari *et al.* 2022). Although ZnO and TiO_2 have similar bandgap energies of 3.37 and 3.2 eV, respectively, the potential of the CB and VB of ZnO is slightly more negative than that of TiO_2 (Suganthi *et al.* 2020). When ZnO is irradiated with photons having energy larger than the bandgap of ZnO electrons get photo excited from VB to CB leaving holes in VB. Because of the potential difference between the CB of ZnO and TiO_2, the electrons get transferred from the CB of ZnO to the CB of TiO_2 and conversely, holes travel from VB of TiO_2 to VB of ZnO under UV excitation (Zha *et al.* 2015). This leads to the efficient charge separation of photogenerated charge carriers

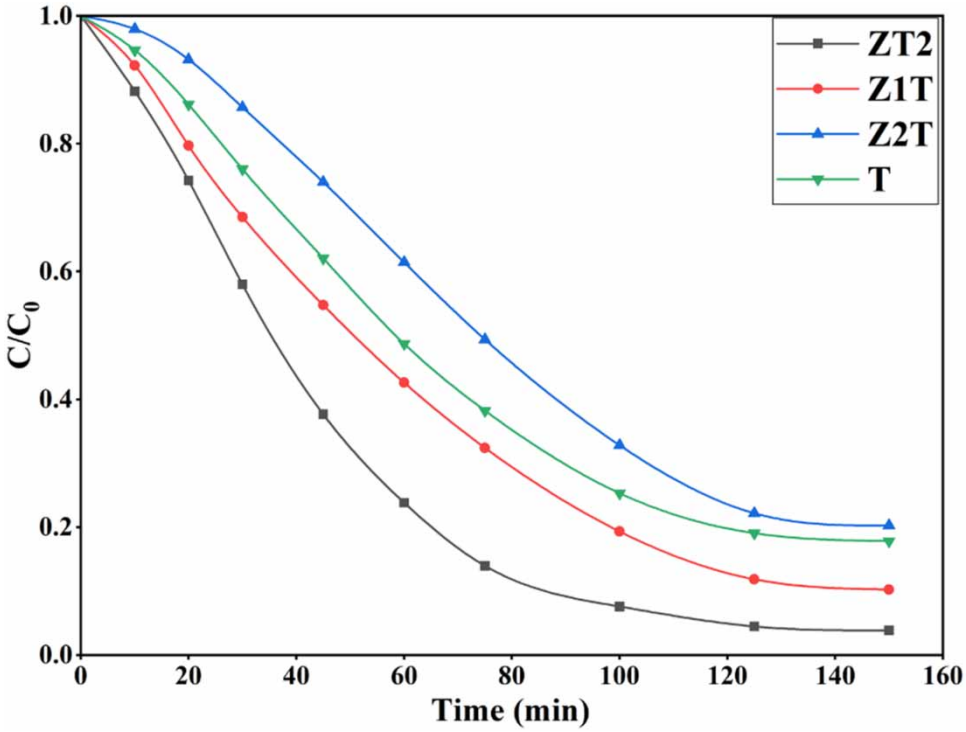

Figure 8 | Photocatalytic decolourisation of MB using TiO_2 and ZnO/TiO_2 with different weight ratios of ZnO.

Table 1 | Kinetic data and percentage efficiency of photocatalytic degradation process

Sample	k_1 (min^{-1})	R^2	% Decolourisation
ZT2	0.02362	0.9911	96.13
Z1T	0.01566	0.9937	89.73
Z2T	0.01054	0.9757	79.66
TiO_2	0.01236	0.9905	82.15

reducing the recombination of photogenerated electron/hole pair. This will enhance the efficiency of interfacial charge transfer to the adsorbed catalyst surface. The heterojunction of ZT2 has a high transport rate of photo-induced electrons and holes, enhancing the pollutants' degradation rate. The combined effect of all of these may be the potential reason for the improved photocatalytic activity of the catalyst with a dose of ZnO (Chattopadhyay *et al.* 2019). As the concentration of ZnO increased the efficiency of photodegradation decreased. ZnO/TiO_2 (2:1) (Z2T) ratio showed the least efficiency among the catalysts, this may be due to the overlapping and saturation of ZnO particles on the active sites of ZnO/TiO_2's composite (Ngo Thi *et al.* 2022). However, a high dose of ZnO may lead to reduced light penetration by the photocatalyst suspension, reducing the degradation rate (Moradi *et al.* 2016). For further ZnO/TiO_2 of weight ratio 1:2 was considered as the optimum catalyst due the higher pollutant removal efficiency.

3.2.2. Effect of catalyst loading on dye removal

To avoid the excessive use of catalysts it is advisable to find the optimum dosage of catalyst for the effective degradation of dyes. To study the effect of catalyst dosing a dye concentration of 8 mg/L and a working volume of 100 mL was taken for both MB and MO. The concentration of the catalyst i.e., ZnO/TiO_2 of weight ratio 1:2 (ZT2) was varied from 60 to 200 mg/L for MB and from 100 to 1,300 mg/L for MO with a time of contact of 150 and 240 min for MB and MO, respectively. Tables 2 and 3 show the kinetic data of photocatalytic degradation of MB and MO for varying catalyst dosage. In Figure 9(a) it can be seen that with the increase in catalyst dosage, the photodegradation rate increased up to a loading of 100 mg/L for MB. MB showed maximum dye degradation within 130 min of contact time with a catalyst dosage of 100 mg/L and reached a stabilised state. When the catalyst dosage for MB was further increased beyond 100 mg/L, it led to the reduction of the photodegradation constant (k) from 0.02379 to 0.02236 min^{-1}. When the catalyst dosage was increased from 100 to 1,000 mg/L the degradation efficiency of MO increased from 32.13 to 89.39%. For MO a maximum removal of 89.39% occurred at 1,000 mg/L with a contact time of 240 minutes. The removal efficiency was reduced to 87.5% when the catalyst loading was further increased to 1,300 mg/L. As the catalyst dosage was increased the degradation rate increased due to an increase in active sites on the surface of the catalyst resulting in greater electron/hole pair for degradation. Above the optimum dosage, the degradation of dye remained almost the same. And when catalyst loading was further increased it led to the reduction in dye degradation. This may be due to the hindrance and blocking of light penetration due to the excessive amount of catalyst particles. Also, particle aggregation is significant at high dosages of catalyst which may lead to the reduction in active sites on the catalyst surface (Habib *et al.* 2013). Hence the optimum dosage of catalyst for MB and MO was taken as 100 and 1,000 mg/L, respectively. MO being an azo dye is more stable and difficult to degrade because of the presence of the azo group, hence MO requires more catalyst dosage and longer contact time than MB for efficient degradation (Waghchaure *et al.* 2022). There was not any discernible decrease in MO or MB concentration during dark

Table 2 | Kinetic data and percentage efficiency of photocatalytic degradation process of MB for varying catalyst dosages

Sample	k_1 (min^{-1})	R^2	% Decolourisation
60 mg/L	0.01434	0.9835	89
100 mg/L	0.02379	0.9916	96.13
200 mg/L	0.02236	0.9904	95.81

Table 3 | Kinetic data and percentage efficiency of photocatalytic degradation process of MO for varying catalyst dosages

Catalyst concentration	k_1 (min^{-1})	R^2	% Decolourisation
100	0.00125	0.9659	32.12
300	0.00242	0.9610	51.96
500	0.00312	0.9764	77.64
800	0.00484	0.9639	89.39
1,000	0.00778	0.9669	87.53

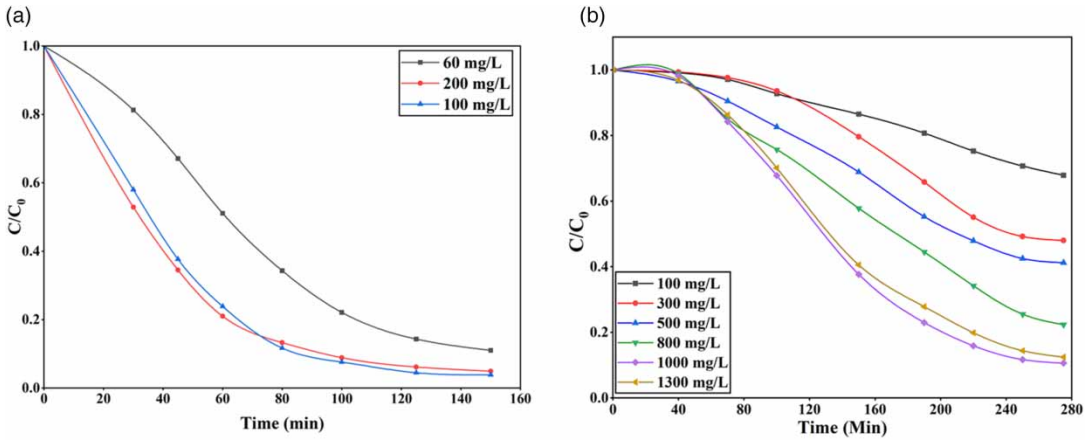

Figure 9 | Photocatalytic degradation of (a) methylene blue and (b) methyl orange using ZT2 composite for different catalyst loading.

adsorption, this may be due to the limited adsorption and activation property of the catalyst in the absence of solar radiation. The same results were reported in the study conducted by (Rashid Al-Mamun *et al.* 2022). It is to be noted that no significant dye decolourisation of MO occurred without a catalyst under solar irradiation indicating that the dye was resistant to self-photolysis in aqueous solution under solar light whereas photolysis removed 40% of MB dye in 150 min without the catalyst.

3.2.3. Effect of initial pH on dye removal

Generally, the pH of the solution plays an important role in the characteristics of wastewater, determines the surface charge properties of catalysts, and affects the adsorption of dye onto the catalyst's surface and the concentration of hydroxyl radicals. MO is an anionic dye and and MB a cationic dye. The adsorption and photocatalytic activity for these dye greatly depend on the pH of the solution (Trabelsi *et al.* 2016). Degradation of MO and MB was carried out at three pH (pH 3, 7, and 11) values to study the effect of pH on the degradation efficiency. The optimum catalyst dosage of both MO and MB was dispersed in 100 mL of 8 mg/L dye solution. MB showed higher degradation in an alkaline medium. In Figure 10, it can be seen that when the pH was

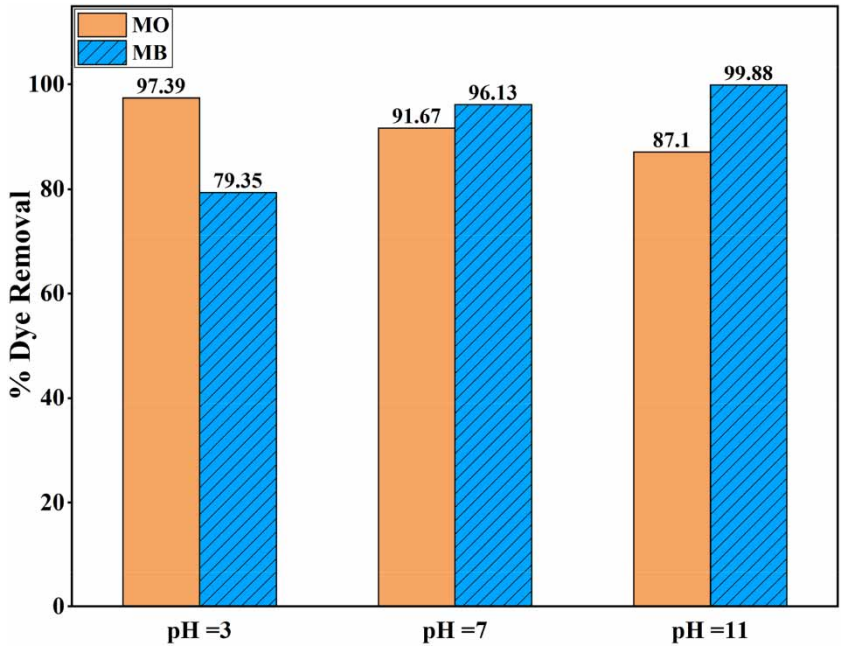

Figure 10 | Dye decolourisation comparison between MB and MO at different initial pH.

increased from 3 to 11 the efficiency of dye removal increased from 79.35 to 99.88%. Whereas for MO, the efficiency of dye removal decreased from 97.39 to 87.10% with an increase in pH from 3 to 11.

The photocatalytic reactions of aqueous ZnO/TiO_2 suspension system can be described as follows (Ge *et al.* 2009):

$$ZnO + h\nu(< 380\ nm) \rightarrow h^+ + e^- \quad (3)$$

$$TiO_2 + h\nu(< 380\ nm) \rightarrow h^+ + e^- \quad (4)$$

$$h^+ + OH^-(surface) \rightarrow OH^\bullet \quad (5)$$

$$h^+ + H_2O \rightarrow OH^\bullet + OH^- \quad (6)$$

$$OH^\bullet + Dye \rightarrow degradation\ products \quad (7)$$

The zero-point charge pH_{zpc} of TiO_2 and ZnO are about 6.8 and 9, respectively (Mostafa *et al.* 2022). At a pH lower or higher than the pH_{zpc}, ZnO/TiO_2 composite is positively or negatively charged, respectively (Habib *et al.* 2013). At acidic pH (pH 2 or pH 6) the composite will be positively charged and the negatively charged MO anions will get adsorbed onto the surface of the catalysts enhancing the degradation of the dye. In alkaline medium ZnO/TiO_2 composite becomes negatively charged and the adsorption of MO anion on the catalyst surface decreases due to Coulomb repulsion between them leading to a reduced degradation rate. In addition, in acidic medium, the photogenerated hole reacts with water to produce hydroxyl radicals as given in Equation (6), which has a strong oxidation capacity to oxidise organic pollutants (Equation (7)) (Ge *et al.* 2009).

MB is a cationic dye, and it does not dissociate into ions in the same way as a salt would. Instead, it exists as a positively charged molecule. The electrostatic interaction between negatively charged composite and positively charged MB results in greater degradation in alkaline medium (Abdellah *et al.* 2018). Also, at higher pH hydroxyl radicals will be formed through the reaction of OH- with photogenerated holes.

3.2.4. Recycling of the catalyst

The lifespan of the catalyst is an important factor in the evaluation of a catalyst (Hernández *et al.* 2015). Photocatalysis may be made more economical by reusing the catalyst (Awais *et al.* 2022). For the reusability study, 8 mg/L of MB dye in 100 mL volume was taken with a catalyst dosage of 200 mg/L with a contact time of 150 min. The reusability study was carried out under solar radiation. After each cycle, the catalyst was filtered using suction filtration. During the filtration process, the catalyst was washed several times with ethanol and deionised water and heated at 110 °C to evaporate moisture. Figure 11 shows the relative reusability of the catalyst ZT2 for the decolourisation of MB up to three cycles. The decolourisation efficiency reduced to 90.2 and 85.5% in the second and third cycle, respectively. It can be clearly stated that the decolourisation efficiency slightly decreased with increase in number of cycles. This indicates that the catalyst had good potential to be recycled. The reduction in decolourisation efficiency may be attributed due to the loss of catalyst recovered after each cycle. Reduced catalyst dosage means reduced number of active sites for photocatalysis. After reuse the adsorption capacity of the catalyst may be decreased, resulting in decreased photocatalytic activity (Awais *et al.* 2022). Fouling of the catalyst by the by-products of degradation can be another reason for the decrease in the decolourisation of MB (Hernández *et al.* 2015). Overall, the minor reduction in decolourisation efficiency suggest that the catalyst possess substantial potential for recycling, presenting an economic advantage.

4. CONCLUSION

In this study, ZnO/TiO_2 composite was synthesised from hibiscus leaf extract by using the green synthesis method. The composites were prepared for different weight ratios of ZnO ($ZnO:TiO_2$ – 1:2, 1:1, and 2:1). Among the three catalysts prepared, ZT2 with a weight ratio of 1:2 showed the maximum efficiency. After 150 min of contact time, under solar radiation, 96.13% of MB was degraded. The degradation rate constant of ZT2 was 1.9 times the degradation rate constant of green synthesised TiO_2 suggesting that the photocatalytic activity of ZnO/TiO_2 composite is better than pure TiO_2 which can be attributed to the formation of heterojunction which effectively separates the photogenerated charge carriers, reducing their recombination. The degradation efficiency of Z2T was less compared to TiO_2, as a higher dose of ZnO to TiO_2 decreases the

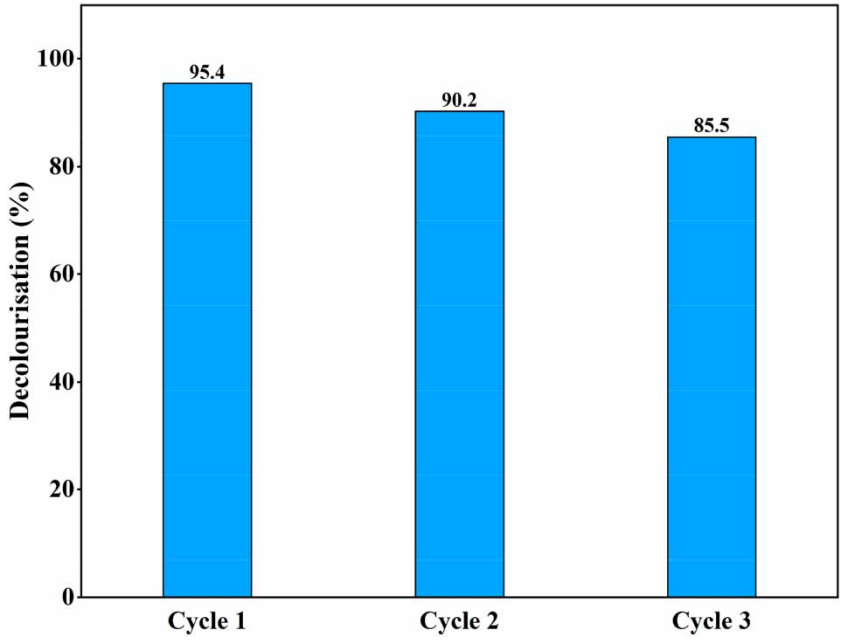

Figure 11 | Reusability of ZT2 catalyst for the decolourisation of MB.

active sites of TiO_2 due to saturation and overlapping, decreasing the degradation rate. The XRD and FTIR characterisation confirmed the formation of ZnO/TiO_2 composite. XRD analysis showed the well-crystallised anatase TiO_2 and wurtzite ZnO. The presence of Zn–O–Ti bond at the broad band 1,800–2,300 cm^{-1} centred at 2,028 cm^{-1} in FTIR analysis indicates that ZnO has been embedded into the surface of TiO_2. FESEM revealed the flaky hexagonal structure of ZnO and reflected the morphology of TiO_2 as a spherical structure. FESEM images of the composite revealed the distribution of ZnO over TiO_2. EDS analysis confirmed the presence of Ti, Zn and O elements in the composite. According to the UV–Vis study, the bandgap of ZT2 and TiO_2 were 2.98 and 3.14 eV, respectively, indicating the formation of heterojunction caused a red shift in the absorption spectrum making the composite more active in the visible region. The photocatalytic activity ZT2 catalyst was evaluated by degrading cationic MB and anionic MO. In addition, factors affecting the degradation of dyes including the catalyst dosage and initial pH were investigated. The optimum catalyst dosage for a dye concentration of 8 mg/L was found to be 100 and 1,000 mg/L for MB and MO, respectively. MB showed maximum degradation at alkaline pH whereas MO showed maximum degradation at acidic pH. Furthermore, the synthesised catalyst ZT2 showed good recyclability. Therefore, ZnO/TiO_2 shows great potential for pollution abatement under solar light.

ACKNOWLEDGEMENTS

The authors thank the Central Research Facility, National Institute of Technology Karnataka, Surathkal, for the facilities provided for material characterisation. K.A. acknowledges Ministry of Education, India for the PG fellowship.

FUNDING

No funding was received for conducting this study.

DATA AVAILABILITY STATEMENT

All relevant data are included in the paper or its Supplementary Information.

CONFLICT OF INTEREST

The authors declare there is no conflict.

REFERENCES

Abd El-Kader, M. F. H., Elabbasy, M. T., Adeboye, A. A., Zeariya, M. G. M. & Menazea, A. A. 2021 Morphological, structural and antibacterial behavior of eco-friendly of ZnO/TiO_2 nanocomposite synthesized via Hibiscus rosa-sinensis extract. *Journal of Materials Research and Technology* **15**, 2213–2220.

Abdellah, M. H., Nosier, S. A., El-Shazly, A. H. & Mubarak, A. A. 2018 Photocatalytic decolorization of methylene blue using TiO_2/UV system enhanced by air sparging. *Alexandria Engineering Journal* **57**(4), 3727–3735.

Akhter, P., Nawaz, S., Shafiq, I., Nazir, A., Shafique, S., Jamil, F., Park, Y. K. & Hussain, M. 2023 Efficient visible light assisted photocatalysis using ZnO/TiO_2 nanocomposites. *Molecular Catalysis* **535**, 112896.

Ali, M. M., Haque, M. J., Kabir, M. H., Kaiyum, M. A. & Rahman, M. S. 2021 Nano synthesis of ZnO–TiO_2 composites by sol-gel method and evaluation of their antibacterial, optical and photocatalytic activities. *Results in Materials* **11**, 100199.

Al-Tohamy, R., Ali, S. S., Li, F., Okasha, K. M., Mahmoud, Y. A. G., Elsamahy, T., Jiao, H., Fu, Y. & Sun, J. 2022 A critical review on the treatment of dye-containing wastewater: Ecotoxicological and health concerns of textile dyes and possible remediation approaches for environmental safety. *Ecotoxicology and Environmental Safety* **231**, 113160.

Awais, M., Khursheed, S., Tehreem, R., Sirajuddin, Mok, Y. S. & Siddiqui, G. U. 2022 Ph regulated rapid photocatalytic degradation of methylene blue dye via niobium-nitrogen co-doped titanium dioxide nanostructures under sunlight. *Applied Catalysis A: General* **643**, 118764.

Bai, N., Liu, X., Li, Z., Ke, X., Zhang, K. & Wu, Q. 2021 High-efficiency TiO_2/ZnO nanocomposites photocatalysts by sol–gel and hydrothermal methods. *Journal of Sol-Gel Science and Technology* **99**(1), 92–100.

Chandrabose, G., Dey, A., Gaur, S. S., Pitchaimuthu, S., Jagadeesan, H., Braithwaite, N. S. J., Selvaraj, V., Kumar, V. & Krishnamurthy, S. 2021 Removal and degradation of mixed dye pollutants by integrated adsorption-photocatalysis technique using 2-D MoS_2/TiO_2 nanocomposite. *Chemosphere* **279**, 130467.

Chattopadhyay, S., Basu, S. & Saha, S. 2019 Solar driven photocatalytic activity of TiO_2 -ZnO nanocomposite. In: *AIP Conference Proceedings*, vol. 2087. American Institute of Physics Inc.

Fendrich, M. A., Quaranta, A., Orlandi, M., Bettonte, M. & Miotello, A. 2018 Solar concentration for wastewaters remediation: A review of materials and technologies. *Applied Sciences (Switzerland)* **9**(1), 118.

Ge, M., Guo, C., Zhu, X., Ma, L., Han, Z., Hu, W. & Wang, Y. 2009 Photocatalytic degradation of methyl orange using ZnO/TiO_2 composites. *Frontiers of Environmental Science and Engineering in China* **3**(3), 271–280.

Habib, A., Shahadat, T., Mohammed Bahadur, N. & Mahmood, A. J. 2013 Synthesis and characterization of ZnO-TiO_2 nanocomposites and their application as photocatalysts. *International Nano Letters* **3**, 1–8.

Hernández, S., Hidalgo, D., Sacco, A., Chiodoni, A., Lamberti, A., Cauda, V., Tresso, E. & Saracco, G. 2015 Comparison of photocatalytic and transport properties of TiO_2 and ZnO nanostructures for solar-driven water splitting. *Physical Chemistry Chemical Physics* **17**(12), 7775–7786.

Jayappa, M. D., Ramaiah, C. K., Kumar, M. A. P., Suresh, D., Prabhu, A., Devasya, R. P. & Sheikh, S. 2020 Green synthesis of zinc oxide nanoparticles from the leaf, stem and in vitro grown callus of Mussaenda frondosa L.: Characterization and their applications. *Applied Nanoscience (Switzerland)* **10**(8), 3057–3074.

Kumari, M. L. A., Devi, L. G., Maia, G., Chen, T. W., Al-Zaqri, N. & Ali, M. A. 2022 Mechanochemical synthesis of ternary heterojunctions TiO_2(A)/TiO_2(R)/ZnO and TiO_2(A)/TiO_2(R)/SnO_2 for effective charge separation in semiconductor photocatalysis: A comparative study. *Environmental Research* **203**, 111841.

Ma, Q. L., Xiong, R., Zhai, B. G. & Huang, Y. M. 2015 Ultrasonic synthesis of fern-like ZnO nanoleaves and their enhanced photocatalytic activity. *Applied Surface Science* **324**, 842–848.

Mbrouk, O., Hafez, H., Mozia, S., Othman, A. M. & Abdel Mottaleb, M. S. A. 2022 Stimulated generation of photobiogas by morphologically tuned nanostructured ZnO and ZnO/TiO_2. *BMC Chemistry* **16**(1), 74.

Mehrabi, M. & Javanbakht, V. 2018 Photocatalytic degradation of cationic and anionic dyes by a novel nanophotocatalyst of TiO_2/$ZnTiO_3$/αFe_2O_3 by ultraviolet light irradiation. *Journal of Materials Science: Materials in Electronics* **29**(12), 9908–9919.

Moradi, S., Aberoomand-Azar, P., Raeis-Farshid, S., Abedini-Khorrami, S. & Givianrad, M. H. 2016 The effect of different molar ratios of ZnO on characterization and photocatalytic activity of TiO_2/ZnO nanocomposite. *Journal of Saudi Chemical Society* **20**(4), 373–378.

Mostafa, N. G., Yunnus, A. F. & Elawwad, A. 2022 Adsorption of Pb(II) from water onto ZnO, TiO_2, and Al_2O_3: Process study, adsorption behaviour, and thermodynamics. *Adsorption Science and Technology* **2022**.

Mousa, H. M., Alenezi, J. F., Mohamed, I. M. A., Yasin, A. S., Hashem, A. F. M. & Abdal-hay, A. 2021 Synthesis of TiO_2@ZnO heterojunction for dye photodegradation and wastewater treatment. *Journal of Alloys and Compounds* **886**, 161169.

Nam, S. H., Cho, S. J. & Boo, J. H. 2012 Growth behavior of titanium dioxide thin films at different precursor temperatures. *Nanoscale Research Letters* **7**, 1–6.

Nandiyanto, A. B. D., Oktiani, R. & Ragadhita, R. 2019 How to read and interpret ftir spectroscope of organic material. *Indonesian Journal of Science and Technology* **4**(1), 97–118.

Ngo Thi, T. D., Nguyen, L. H., Nguyen, X. H., Phung, H. V., The Vinh, T. H., Viet, P. V., Thai, N. V., Le, H. N., Pham, D. T., Van, H. T., Than Thi, L. H., Pham Thi, T. D., Minh, T. L., Phan Quang, H. H., Nguyen Vu, H. P., Duc, T. T. & Nguyen, H. M. 2022 Enhanced heterogeneous photocatalytic perozone degradation of amoxicillin by ZnO modified TiO2 nanocomposites under visible light irradiation. *Materials Science in Semiconductor Processing* **142**, 106456.

Rashid Al-Mamun, M., Hossain, K. T., Mondal, S., Afroza Khatun, M., Shahinoor Islam, M. & Zaved Hossain Khan, D. M. 2022 Synthesis, characterization, and photocatalytic performance of methyl orange in aqueous TiO_2 suspension under UV and solar light irradiation. *South African Journal of Chemical Engineering* **40**, 113–125.

Sadiq, H., Sher, F., Sehar, S., Lima, E. C., Zhang, S., Iqbal, H. M. N., Zafar, F. & Nuhanović, M. 2021 Green synthesis of ZnO nanoparticles from Syzygium Cumini leaves extract with robust photocatalysis applications. *Journal of Molecular Liquids* **335**, 116567.

Sethy, N. K., Arif, Z., Mishra, P. K. & Kumar, P. 2020 Green synthesis of TiO2 nanoparticles from Syzygium cumini extract for photo-catalytic removal of lead (Pb) in explosive industrial wastewater. *Green Processing and Synthesis* **9**(1), 171–181.

Soto-Robles, C. A., Luque, P. A., Gómez-Gutiérrez, C. M., Nava, O., Vilchis-Nestor, A. R., Lugo-Medina, E., Ranjithkumar, R. & Castro-Beltrán, A. 2019 Study on the effect of the concentration of Hibiscus sabdariffa extract on the green synthesis of ZnO nanoparticles. *Results in Physics* **15**, 102807.

Suganthi, N., Thangavel, S. & Kannan, K. 2020 Hibiscus subdariffa leaf extract mediated 2-D fern-like ZnO/TiO_2 hierarchical nanoleaf for photocatalytic degradation. *FlatChem* **24**, 100197.

Trabelsi, H., Atheba, G. P., Hentati, O., Dezirée Mariette, Y., Robert, D., Drogui, P. & Ksibi, M. 2016 Solar photocatalytic decolorization and degradation of methyl orange using supported TiO_2. *Journal of Advanced Oxidation Technologies* **19**(1), 79.

Tumbelaka, R. M., Istiqomah, N. I., Kato, T., Oshima, D. & Suharyadi, E. 2022 High reusability of green-synthesized Fe_3O_4/TiO_2 photocatalyst nanoparticles for efficient degradation of methylene blue dye. *Materials Today Communications* **33**, 104450.

Waghchaure, R. H., Adole, V. A. & Jagdale, B. S. 2022 Photocatalytic degradation of methylene blue, rhodamine B, methyl orange and Eriochrome black T dyes by modified ZnO nanocatalysts: A concise review. *Inorganic Chemistry Communications* **143**, 109764.

Zha, R., Nadimicherla, R. & Guo, X. 2015 Ultraviolet photocatalytic degradation of methyl orange by nanostructured TiO_2/ZnO heterojunctions. *Journal of Materials Chemistry A* **3**(12), 6565–6574.

First received 13 October 2023; accepted in revised form 19 January 2024. Available online 2 February 2024